J Ginseng Res 44 (2020) 341–349

Contents lists available at ScienceDirect

Journal of Ginseng Research

journal homepage: http://www.ginsengres.org

Research Article

Stereoisomer-specific ginsenoside 20(*S*)-Rg3 reverses replicative senescence of human diploid fibroblasts via Akt-mTOR-Sirtuin signaling

Kyeong-Eun Yang [1,☆], Hyun-Jin Jang [1,2,☆], In-Hu Hwang [3], Eun Mi Hong [1], Min-Goo Lee [4], Soon Lee [5], Ik-Soon Jang [1,5,*], Jong-Soon Choi [1,6,*]

[1] *Biological Disaster Analysis Group, Korea Basic Science Institute, Daejeon, Republic of Korea*
[2] *Department of Biological Sciences, Sungkyunkwan University, Suwon, Republic of Korea*
[3] *Neuroscience Research institute, Korea University College of Medicine, Seoul, Republic of Korea*
[4] *Department of Physiology, Korea University College of Medicine, Seoul, Republic of Korea*
[5] *Division of Bio-Analytical Science, University of Science and Technology, Daejeon, Republic of Korea*
[6] *Graduate School of Analytical Science and Technology, Chungnam National University, Daejeon, Republic of Korea*

ARTICLE INFO

Article history:
Received 13 February 2019
Received in Revised form
1 August 2019
Accepted 7 August 2019
Available online 13 August 2019

Keywords:
Akt-mTOR-sirtuin signaling
Ginsenoside Rg3(*S*)
Human dermal fibroblast
Reversal
senescence

ABSTRACT

Background: The replicative senescence of human dermal fibroblasts (HDFs) is accompanied by growth arrest. In our previous study, the treatment of senescent HDFs with Rg3(*S*) lowered the intrinsic reactive oxygen species (ROS) levels and reversed cellular senescence by inducing peroxiredoxin-3, an antioxidant enzyme. However, the signaling pathways involved in Rg3(*S*)-induced senescence reversal in HDFs and the relatedness of the stereoisomer Rg3(*R*) in corresponding signaling pathways are not known yet.
Methods: We performed senescence-associated β-galactosidase and cell cycle assays in Rg3(*S*)-treated senescent HDFs. The levels of ROS, adenosine triphosphate (ATP), and cyclic adenosine monophosphate (cAMP) as well as the mitochondrial DNA copy number, nicotinamide adenine dinucleotide $(NAD)^+$/1,4-dihydronicotinamide adenine dinucleotide (NADH) ratio, and NAD-dependent sirtuins expression were measured and compared among young, old, and Rg3(*S*)-pretreated old HDFs. Major signaling pathways of phosphatidylinositol 3-kinase/Akt, 5' adenosine monophosphate-activated protein kinase (AMPK), and sirtuin 1/3, including cell cycle regulatory proteins, were examined by immunoblot analysis.
Results: Ginsenoside Rg3(*S*) reversed the replicative senescence of HDFs by restoring the ATP level and NAD^+/NADH ratio in downregulated senescent HDFs. Rg3(*S*) recovered directly the cellular levels of ROS and the NAD^+/NADH ratio in young HDFs inactivated by rotenone. Rg3(*S*) mainly downregulated phosphatidylinositol 3-kinase/Akt through the inhibition of mTOR by cell cycle regulators like p53/p21 in senescent HDFs, whereas Rg3(*R*) did not alter the corresponding signaling pathways. Rg3(*S*)-activated sirtuin 3/PGC1α to stimulate mitochondrial biogenesis.
Conclusion: Cellular molecular analysis suggests that Rg3(*S*) specifically reverses the replicative senescence of HDFs by modulating Akt-mTOR-sirtuin signaling to promote the biogenesis of mitochondria.
© 2019 The Korean Society of Ginseng, Published by Elsevier Korea LLC. This is an open access article under the CC BY-NC-ND license (http://creativecommons.org/licenses/by-nc-nd/4.0/).

1. Introduction

Cellular senescence has been known as an irreversible process of cell-cycle arrest, which demonstrates the cessation of cellular division, accompanied by altered cellular morphology, senescence-associated heterochromatin foci, and tumor-suppressor activation [1]. In general, somatic cells such as fibroblasts, melanocytes, and endothelial cells experience the process of definite division termed the “Hayflick limit” as a characteristic of replicative senescence [2]. The main cause of induction of replicative senescence was considered oxidative stressors such as reactive oxygen species (ROS), in which intracellular antioxidant systems can prevent

* Corresponding authors: Biological Disaster Analysis Group, Korea Basic Science Institute, Daejeon 34133, Republic of Korea.
E-mail addresses: jangiksn@kbsi.re.kr (I.-S. Jang), jschoi@kbsi.re.kr (J.-S. Choi).
☆ These authors contributed equally to this work.

https://doi.org/10.1016/j.jgr.2019.08.002
p1226-8453 e2093-4947/$ – see front matter © 2019 The Korean Society of Ginseng, Published by Elsevier Korea LLC. This is an open access article under the CC BY-NC-ND license (http://creativecommons.org/licenses/by-nc-nd/4.0/).

cellular damage from ROS attack [3]. Thus, the balance between the external ROS level and the internal scavenging system is critical to determine whether replicative senescence acts as accelerating or mitigating the aging progress further. For the attenuation of ROS-mediated aging processes in skin and brain, there are many attempts of dietary polyphenols or flavonoids to improve health by enhancing cellular redox capability [4,5]. Likewise, ginseng saponins of *Panax ginseng* Meyer decrease intracellular ROS levels to alleviate oxidative stress, resulting in protection from cellular damage [6,7].

Ginsenoside Rg3, enriched from steamed or heated ginseng roots, exerts multiple pharmacological effects through anti-angiogenic, antitumor, and antidiabetic activities [8]. Rg3 displays two stereoisomeric forms: Rg3(*S*) and Rg3(*R*) based on a chiral center at position C-20. Although the working mechanism of stereoisomeric Rg3 remains clarified, it has been suggested that the stereoisomeric structures of the protopanaxadiol backbone attached to hydroxyl groups on C-20 of Rg3 exert different binding affinities to peroxisome proliferator-activated receptor gamma [9]. Ginsenoside Rg3(*S*) has stronger antidiabetic activity, whereas Rg3(*R*) has more powerful antioxidant activity to promote the immune response in vascular smooth muscle cells [10,11]. However, the stereoisomer Rg3(*S*) decreases the UV-B–induced ROS levels in human dermal fibroblasts (HDFs), but Rg3(*R*) does not exert scavenging activity [12]. Thus, it is notable that the stereospecificity of Rg3 demonstrates antioxidant activity in specific cell types.

The production of intracellular free radicals linked to mitochondrial ROS generation concerns the deteriorated mitochondrial dysfunction and biogenesis, leading to global cellular damage. Mitochondrial dysfunction caused by free radical production directs the perturbation of intracellular signaling or intercellular crosstalk [13]. Thus, the reduced mitochondrial biogenesis may result from the cell cycle regulator p53-mediated suppression of transcriptional coactivator peroxisome proliferator activated receptor gamma coactivator 1 alpha (PGC1α) [14]. Mitochondrial biogenesis induction by PGC1α may be regulated by Sirt1 and mitochondrial-type Sirt3 [15]. Sirt3 is known to be a major mitochondrial regulatory enzyme, which controls the production rate of ROS [16]. In addition, sirtuins control the organic processes via activation of the upstream phosphatidylinositol 3-kinase (PI3K)-Akt signaling pathway during the aging process, accompanied by oxidative stress [17]. Recently, it was reported that antibiotic-induced mitochondrial dysfunction is involved in the suppression of the 5' adenosine monophosphate-activated protein kinase (AMPK)/mTOR/p70S6K pathway and autophagy in fibroblasts [18]. Thus, the cellular senescence induced by ROS is possibly linked to aging-related signaling pathways in HDFs.

In our previous study, the ginsenoside Rg3(*S*) increased the expression of the antioxidant enzyme peroxiredoxin 3 in senescent HDF cells by proteomic analysis [19]. However, the mechanism of Rg3(*S*) action in signaling pathways remains to be elucidated. In the present study, the changes in senescent HDFs during the treatment with Rg3(*S*) or Rg3(*R*) were monitored with the signaling pathways of the Akt-mTOR-sirtuin axis by immunoblot analysis. Together with senescence-associated β-galactosidase (SA-β-gal) activity and flow cytometric cell cycle analysis, biochemical properties such as ROS, adenosine triphosphate (ATP), cyclic adenosine monophosphate (cAMP), nicotinamide adenine dinucleotide $(NAD)^+$/1,4-dihydronicotinamide adenine dinucleotide (NADH) ratio, and mitochondrial copy number will be examined in Rg3(*S*)-pretreated senescent HDFs. These cellular molecular analyses will be helpful in understanding the mechanism of which Rg3(*S*) reverses replicative senescence due to aging.

2. Materials and methods

2.1. Reagents and chemicals

Dulbecco's Modified Eagles Medium (DMEM) was purchased from Sigma Chemical (St. Louis, MO). Chemicals such as fetal bovine serum, penicillin-streptomycin, and phosphate-buffered saline (PBS) were obtained from Gibco (Paisley, Scotland). Stereoisomers ginsenoside 20(*S*) and 20(*R*)-Rg3 (purity >98%) were purchased from the Ambo Institute (Daejeon, Korea). Cell Counting Kit-8 and Senescence Cells Histochemical Staining kit were supplied by Dojindo (Dojindo, Japan) and Sigma Chemical, respectively. Cell culture dishes were purchased from NUNC (Roskilde, Denmark). The whole cell lysis buffer used was PRO-PREP protein extraction solution (iNtRON Biotechnology, Korea).

2.2. Cell culture and treatment

HDFs were obtained from Seoul National University (SNU) and cultured in DMEM-supplemented with 10% (v/v) fetal bovine serum and 1% (w/v) penicillin-streptomycin at 37°C in a 5% (v/v) CO_2 humidified atmosphere. HDFs were maintained until different passages: passage #8-12 (young cells) and passage #34-36 (senescent cells). Senescent HDFs were starved with serum-free DMEM overnight and then incubated in DMEM containing 10 or 30 μM Rg3(*S*) or (*R*) for 48 h.

2.3. Senescence-associated β-galactosidase assay

Expression of SA-β-gal was detected by Senescence Cells Histochemical Staining kit (Sigma) according to the previous study [20]. Briefly, cells were seeded at a density of 2.5×10^4 cells/well in 12-well plates. Rg3(*S*)-treated senescent HDFs were first fixed for 6–7 min at room temperature in fixation buffer. Cells were then washed with PBS and stained with β-gal staining solution for 9 h at 37°C without CO_2. Stained cells were viewed under a microscope at × 100 magnification, and at least three independent experiments were performed. The degree of SA-β-gal positive cells was calculated as a percentage of the total number of cells from five randomly chosen fields.

2.4. Cell cycle analysis with flow cytometry

Cell cycle assay was performed to determine the cell cycle stage with a NucleoCounter NC-3000™ kit (Chemometec, France), according to the manufacturer's instruction. Briefly, senescent cells were incubated with Rg3(*S*) for 48 h, and cells were harvested by trypsinization. Cells were washed once with PBS, fixed with 70% ethyl alcohol for at least 2 h, and centrifuged at 1,400 rpm for 5 min. Cells were then incubated with 4′,6-diamidino-2-phenylindole (DAPI) solution for 5 min at 37°C. DAPI-stained cells were measured in NucleoCounter NC-3000™ at 365 nm, and data were analyzed by NucleoView NC-3000 software.

2.5. Measurement of reactive oxygen species

Intracellular ROS were detected using the fluorescent probe 5-(and 6)-carboxy-2′,7′-dichloro dihydrofluorescein diacetate (DCF-DA) (Sigma) as described previously [21]. HDFs were seeded in 96-well plates, and senescent HDFs were treated with Rg3(*S*) for 48 hr. Subsequently, cells were incubated with 10 μM DCF-DA in darkness for 30 min. After cells were washed with PBS, DCF-DA green fluorescence was measured at 490 nm excitation wavelength and at

535 nm emission wavelength using SpectraMax-M4 (Molecular Devices, Sunnyvale, CA).

2.6. Measurement of ATP, cAMP, and NAD$^+$/NADH ratio

Detection of cellular ATP levels was performed using ATP Colorimetric/Fluorometric Assay kit (BioVision, Milpitas, CA) according to the manufacturer's instructions. Briefly, 1×10^6 Rg3(*S*)-treated senescent HDFs were lysed with ATP assay buffer. The lysates were centrifuged at 13,000 rpm for 2 min at 4°C. After this, supernatants were collected, and 50 μL samples were transferred to a 96-well plate. A reaction mixture of 50 μL was added to each well, and each sample was mixed thoroughly. The plate was incubated in darkness at room temperature for 30 min, and the absorbance was measured at 570 nm using TriStar2 LB 942 (Berthold, Bad Wilbad, Germany). The levels of cAMP were determined using HTRF® cAMP dynamic 2 assay kit (Cisbio, Bedford, MA). Senescent HDFs were stimulated with Rg3(*S*) for 30 min at 37°C. Subsequently, cells were incubated with anti-cAMP cryptate and cAMP-d2 in lysis buffer for 1 h at 37°C. The fluorescence signals were measured at 665 nm and 620 nm using TriStar2 LB 942 (Berthold, Bad Wilbad, Germany). NAD$^+$ and NADH levels were measured with NAD$^+$/NADH Quantitation Colorimetric Kit (BioVision, Milpitas, CA) according to the manufacturer's instructions. Briefly, senescent HDFs were incubated with Rg3(*S*) for 48 h, and cells were harvested by trypsinization. Pellets of 2×10^5 cells were extracted with 400 μL NADH/NAD extraction buffer by two freeze/thaw cycles of 20 min on dry ice and kept for 10 min at room temperature. The extract was centrifuged at 14,000 rpm for 5 min, and the supernatants were collected. For the determination of NADH, NAD$^+$ was degraded by heating at 60°C for 30 min. Samples were incubated with Reaction Mix for 5 min, 10 μL of NADH developer was added, and then were allowed to cycle for 4 hr. Absorbance was measured every hour at 450 nm. NAD$^+$ level was inferred to be the difference between NAD^T (total NADH and NAD$^+$) and NADH.

2.7. Measurement of mitochondrial DNA copy number

The mitochondrial DNA (mtDNA) copy number of HDFs was measured by real-time polymerase chain reaction with Human Mitochondrial DNA Monitoring Primer Set (Takara, Seoul, Korea). Total mtDNA from HDFs (young, senescent, and Rg3(*S*)-pretreated senescent cells) was extracted with Mitochondrial DNA Isolation Kit (BioVision, Milpitas, CA), as described previously [22]. Then, mtDNA was enriched with Agencourt AMPure XP system (Beckman Coulter, Brea, CA) and subjected to polymerase chain reaction quantification using MightyAmp™ for Real Time (TB GreenTM Plus, Takara, Seoul, Korea). The relative quantification of either senescent HDFs or Rg3(*S*)-pretreated senescent HDFs divided by young HDFs was calculated using the formula relative quantification $= 2^{(-\Delta\Delta Ct)}$ and finally expressed as copy numbers of mtDNA.

2.8. Immunoblot analysis

After pretreatment with stereoisomeric Rg3(*S*) or (*R*), cells were harvested by scrapping, collected by centrifugation at 1,200 rpm for 5 min at 4°C, and washed twice with PBS. The resulting cell pellets were resuspended with PRO-PREP protein extraction solution (iNtRON Biotechnology, Sungnam, Korea) and placed on ice for 20 min. The lysates were centrifuged at 13,000 rpm for 20 min at 4°C, and protein concentration of the supernatants was determined using a Pierce BCA protein assay kit (Thermo Scientific, Rockford, IL). Equal amounts of protein from each sample were resolved on sodium dodecyl sulfate (SDS)-Polyacrylamide gel electrophoresis (PAGE) gel and transferred onto nitrocellulose membrane (Pall, Pensacola, FL). Membranes were blocked with 5% (w/v) skimmed milk or Bovine serum albumin (BSA) in Tris buffered saline (TBS)-Tween 20 for 1 h at room temperature, then probed with primary antibodies in blocking buffer overnight at 4°C. In the present study, the primary antibodies were listed in Supplementary Table 1. Membranes were washed three times for 10 min with TBS-Tween 20. Membranes were then incubated with HRP-conjugated goat anti-mouse IgG or HRP-conjugated goat anti-Rabbit IgG in 5% skimmed milk in TBS-Tween 20 at room temperature for 1 h. After three washes with TBS-Tween 20, the immunoreactive proteins were visualized by ECL system (BioFact, Daejeon, Korea), before protein band detection with ImageQuant LAS 4000 mini system (GE Healthcare Life Sciences, Glattbrugg, Switzerland). Protein bands were quantified by densitometry using Image J software, version 1.42 (National Institutes of Health, Bethesda, MD, USA) and normalized with β-actin band density as a loading control.

2.9. Statistical analysis

Each experiment was repeated at least three times. Statistical analysis was performed using a Student *t* test with Graph-Pad Prism (GraphPad, San Diego, CA). Data were expressed as means ± standard deviation. Statistical *P* values of less than 0.05 or 0.01 were considered as significant.

3. Results and discussion

3.1. Rg3(S) reverses the replicative senescence of HDFs

We examined the senescent state of old HDFs at passage #35 and compared the results with those of young HDFs at passage #10 using SA-β-gal staining. Less than 5% of young HDFs were positive for β-galactosidase activity, whereas 80% of old HDFs revealed β-galactosidase-positive cells (Fig. 1A and B). The percentage of SA-β-gal-stained cells in old HDFs given by SNU was double to that in cells purchased from ATCC. However, the percentages of cells of SA-β-gal staining in old HDFs pretreated with Rg3(*S*) of 10 μM and 30 μM for 48 h were significantly decreased to 48% and 38%, respectively. The partial reversion of senescent HDFs by Rg3(*S*) was very similar to our previous observation except for the different origins of HDFs: the cells used in this study were a gift from SNU, and the ones used in the previous study were purchased from ATCC. The stereoisomer Rg3(*R*) showed little effect on the reversal of replicative senescence in the same SA-β-gal staining experiment (data not shown). The phenotypes observed in the SA-β-gal staining were very well matched with those in our previous work.

Next, we examined the alterations to the cell cycle by staining cells with propidium iodide and analyzing cell states using flow cytometry. Propidium iodide−stained old HDFs were compared with Rg3(*S*)-pretreated old HDFs as well as young HDFs. Percentage gating for each fraction was compared among HDF groups. The percentages of natural senescence (the number of cells in sub-G1 fraction) increased from 22% in young HDFs to 36.9% in old HDFs. Contrarily, the percentage of G1 phase cells decreased from 55.1% in young HDFs to 36.9% in old HDFs. Additionally, the percentage fractions of S state were kept constant from 7.7% in young HDFs to 7.8% in old HDFs. These data imply that the senescent old HDFs were arrested at the stage of sub-G1 (G0 and early G1) after the cell division (Fig. 2. Young vs. Old). These data agree with previous study that the senescent fibroblasts were arrested at G1 phase of cell cycle with the increased expression of p16 in G0 and p21 in early G1 phase [23]. However, the senescent old HDFs with Rg3(*S*) dramatically decreased sub-G1 phase from

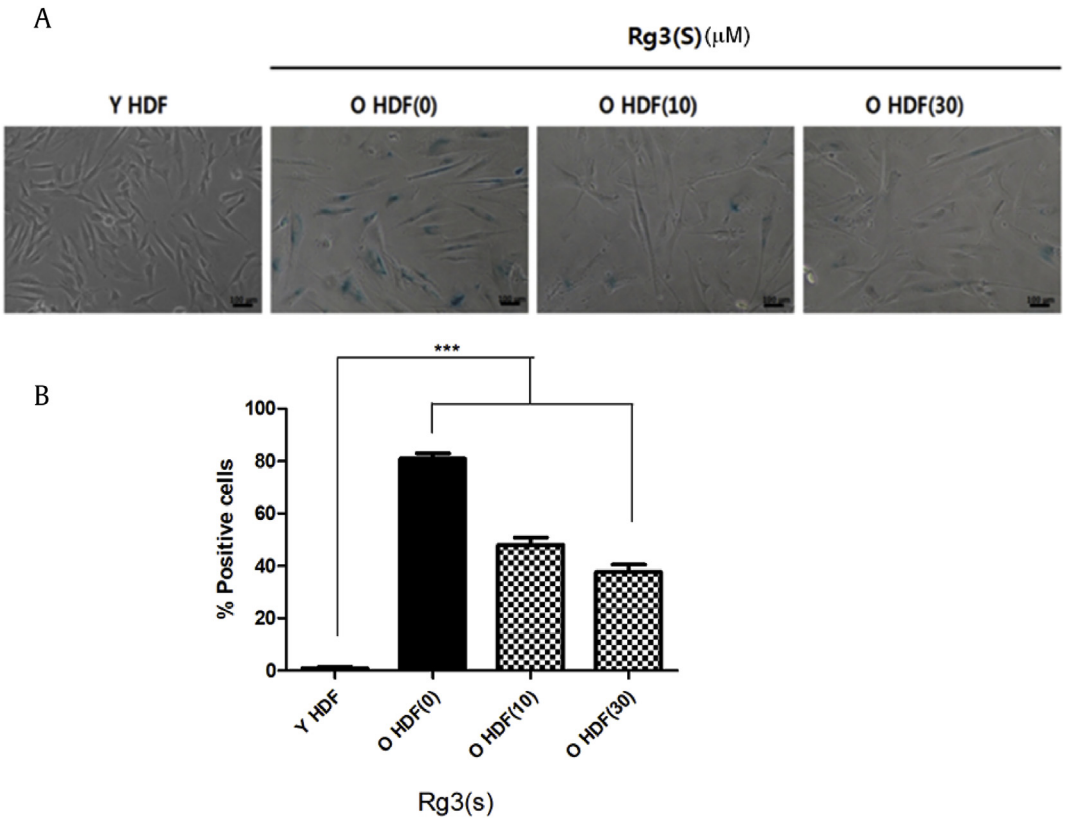

Fig. 1. Senescence-β-galactosidase activity assay of Rg3(*S*)-treated senescent HDFs. (A) Light microscopic images of young HDFs (passage #10) and old HDFs (passage #35) pretreated with 10 μM and 30 μM Rg3(*S*) for 48 h at 37°C. (B) Quantification of SA-β-gal-% positive cells of young and Rg3(*S*)-treated old HDFs. The percentages of SA-β gal-positive cells were calculated by SABIA (eBiogen, Seoul, Korea) using optical microscopy images. Data represent the mean ± SD of three independent experiments. ***Statistical significance $p < 0.001$. HDF, human dermal fibroblast; SA-β-gal, senescence-associated β-galactosidase; SD, standard deviation.

37% to 18% and S-phase from 7.8% to 10~14% (Fig. 2. Old vs. Old + Rg3(*S*)). This suggests that Rg3(*S*) protects old HDFs from cell death and cell cycle arrest at sub-G1 phase after cell division and enhances the rate of cell cycle progression for DNA synthesis at S-phase. Likewise, ginsenoside Rg1 enhanced the resistance of hematopoietic stem and progenitor cells to radiation-induced senescence in mice by regulating the cell cycle [24]. It has been known that the total proteins extracted from *P. ginseng* can promote cell cycle progression in NIH/3T3 cells [25].

3.2. Rg3(S) increases ATP, NAD$^+$/NADH ratio, and sirtuin expression in senescent HDFs

To confirm whether Rg3(*S*) regulates the ROS, ATP, and cAMP content in old HDFs, we measured the intracellular ROS levels and the amounts of ATP and cAMP in HDFs. In agreement with our previous experiment, Rg3(*S*) significantly decreased the levels of ROS in old HDFs provided from SNU (Fig. 3A). Similarly, it was reported that *P. ginseng* calyx ethanol extract had skin-protective

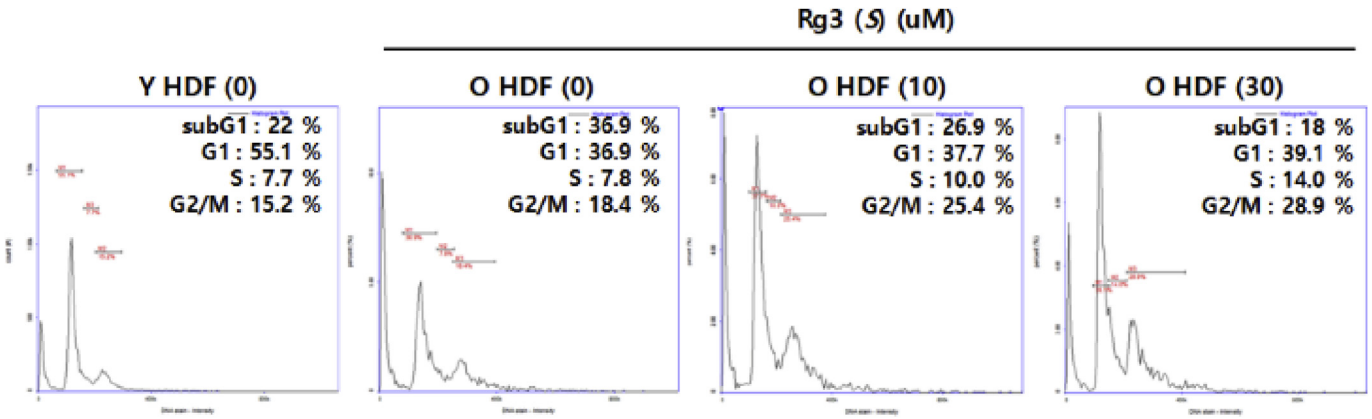

Fig. 2. Flow cytometric analysis of cell cycle. Old HDF cells were pretreated with either vehicle or Rg3(S) (10 μM or 30 μM) for 48 h. Old HDFs were stained with PI and then compared with young HDFs. Percentages of cells in sub-G1, G1, S, and G2/M phases are given in each graph. HDF, human dermal fibroblast; PI, propidium iodide.

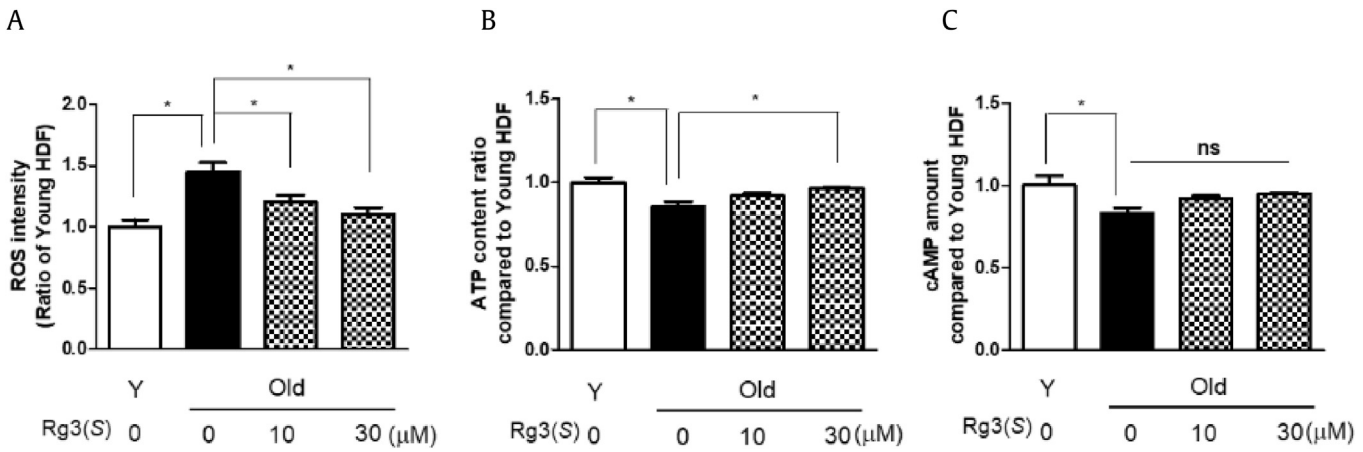

Fig. 3. Levels of ROS, ATP, cAMP in Rg3(*S*)-treated senescent HDFs. (A) ROS, (B) ATP, (C) cAMP levels were measured in young and Rg3(*S*)-treated old HDFs as described in Materials and Methods. Cells were stained with dichlorofluorescein diacetate, fixed, and immediately analyzed using a multi-analytic validation system (SpectraMax M4). The data represent the mean ± SD of three independent experiments. *Statistical significance $p < 0.05$, ** $p < 0.01$, NS : No Significance ROS, reactive oxygen species; SD, standard deviation; HDF, human dermal fibroblast.

properties through protection against H_2O_2-induced damage [26]. In addition, Rg3(*S*) induced ATP level in old HDFs at $p < 0.05$; however, Rg3(*S*) did not alter the level of cAMP (Fig. 3B and C). Collectively, these data indicate that Rg3(*S*) decreases the level of intracellular ROS, irrespective of the origins of HDFs, and Rg3(*S*) increases the levels of ATP level, not cAMP, through the activation of mitochondrial functions. These data are well matched with the recent study that the senescent state was linked to a decrease in the ratio of ATP to ADP and AMP, suggesting a metabolic shift as a preferential use of glycolytic metabolism [27–29]. As to the recovery of ATP content in old HDFs by Rg3(*S*) in our study, it was similarly reported that the ginsenoside Rg1 pretreatment significantly attenuated the decline of ATP in induced senescent fibroblasts [30].

Mitochondria play key roles of ATP generation, NA*D/NADH metabolism, and cellular processes such as signaling pathways, cell

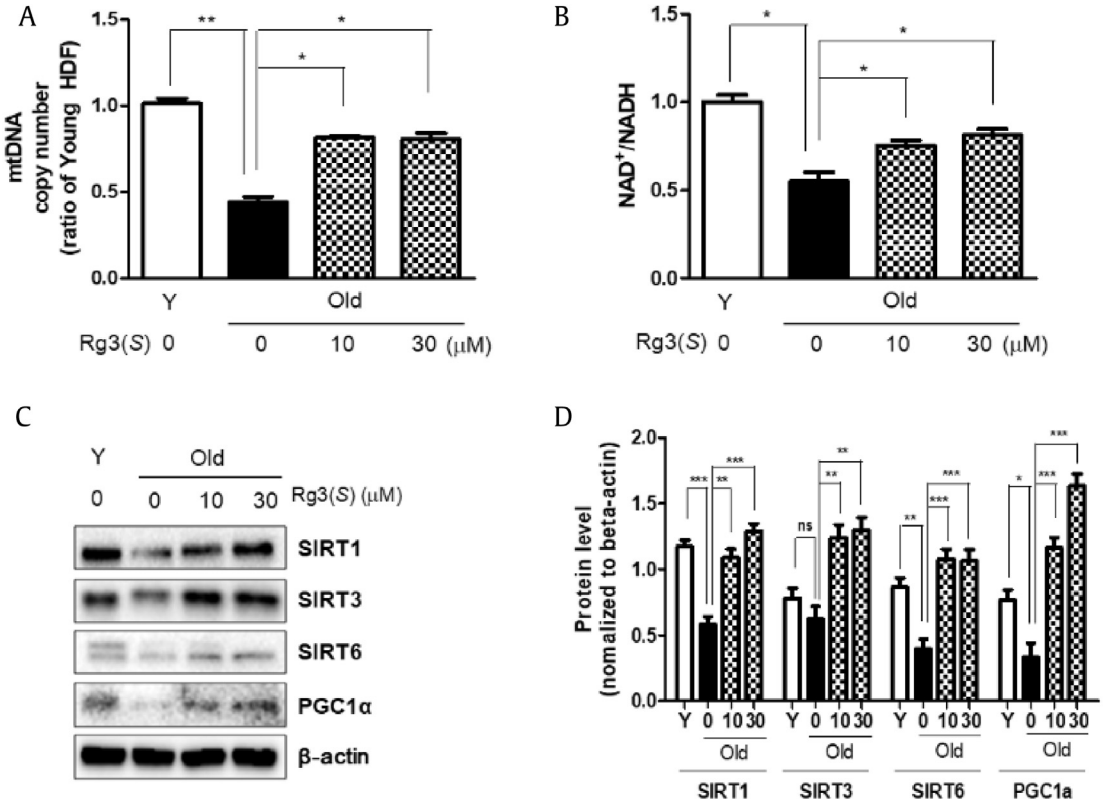

Fig. 4. Measurement of mitochondrial DNA copy number and NAD^+/NADH ratio in Rg3(*S*)-treated senescent HDFs. (A) Mitochondrial copy numbers and (B) NAD^+/NADH ratios were measured as described in Materials and Methods. (C) Immunoblot of sirtuins and PGCα levels in Rg3(*S*)-treated old HDFs. To compare relative expression levels, β-actin was used as loading control. (D) Quantification of protein expression levels was performed using Image J. Statistical significance: *ns*, not significant, $^*p < 0.05$, $^{**}p < 0.01$, $^{***}p < 0.001$. HDF, human dermal fibroblast.

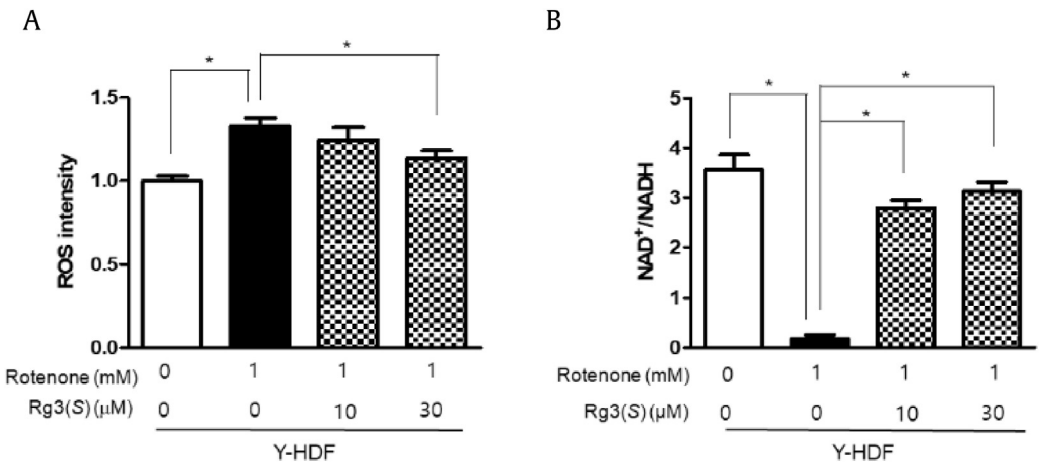

Fig. 5. Rotenone-induced ROS levels and NAD$^+$/NADH ratios in Rg3(*S*)-treated young HDFs. (A) ROS levels and (B) NAD+/NADH ratios in rotenone-pretreated young HDFs. Cells were stained with dichlorofluorescein diacetate, fixed, and immediately analyzed using a multianalytic validation system (SpectraMax M4). The data represent the mean ± SD of three independent experiments. *Statistical significance: $p < 0.05$, ** $p < 0.01$. ROS, reactive oxygen species; SD, standard deviation; HDF, human dermal fibroblast.

growth/differentiation, cell cycle, and cell death [31]. Thus, to assess the activities of mitochondria in HDFs, we measured the mtDNA copy number as an indicator of mitochondrial biogenesis. As shown in Fig. 4A, the mitochondrial copy number in old HDFs was decreased to 45% in young HDFs. However, Rg3(*S*) increased the mitochondrial content to approximately two-fold upon the dose of 10 or 30 μM in old HDFs. Moreover, the intracellular NAD$^+$/NADH ratios in old HDFs decreased by up to 50% compared with that of young HDFs. Interestingly, Rg3(*S*) stimulated the NAD$^+$/NADH ratio to recover to 40~60% levels in old HDFs when Rg3(*S*) of 10 or 30 μM was pretreated in old HDFs (Fig. 4B). Subsequently, we demonstrated whether sirtuins and PGC1α are activated to induce mitochondrial biogenesis in old HDFs treated with Rg3(*S*). As shown in Fig. 4C, the levels of sirtuins such as Sirt1, Sirt3, and Sirt6 and PGC1α as a transcriptional regulator of mitochondria were increased in Rg3(*S*)-stimulated old HDFs. In particular, the increases of Sirt1 and PGC1α were observed in a dose-dependent manner. In addition, the expression of Sirt3 and Sirt6 was saturated in 10 μM Rg3(*S*) pretreated in old HDFs (Fig. 4D). Likewise, Rg3(*S*) was known as a potential Sirt1 activator and to increase the NAD$^+$/NADH ratio in HEK293 cells [32]. Rb1 was known to stimulate Sirt1 to protect Human umbilical vein endothelial cells (HUVECs) from senescence [33]. In addition, it is known that Rg3 improves mitochondrial function and biogenesis by restoring ATP and PGC1α levels in C2C12 cells [34]. In context with related studies, our finding that Rg3(*S*) stimulates sirtuin-1, sirtuin-3, and sirtuin-6 and AMPK to

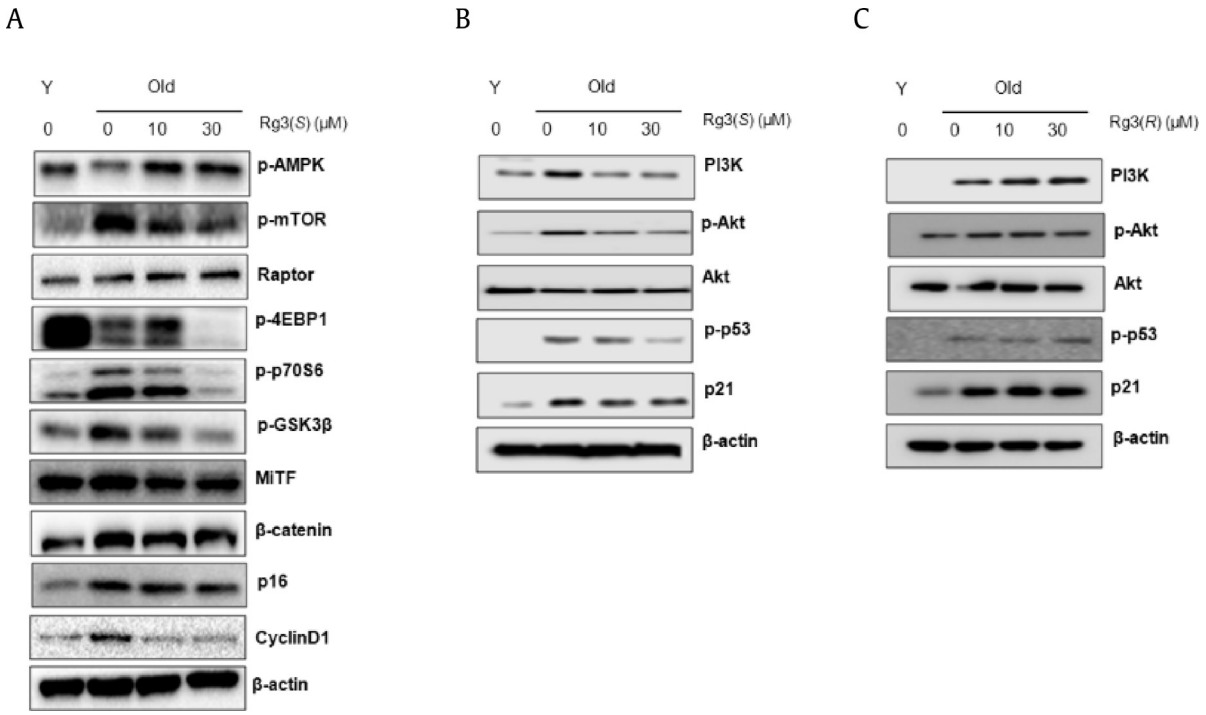

Fig. 6. Immunoblot analysis of Akt, mTOR, and cell cycle regulators in Rg3(*S*)-treated senescent HDFs. (A) The expression levels of mTOR, AMPK, regulators of MiTF expression, and cell cycle arrest proteins were measured using immunoblot. PI3K, Akt, and cell cycle regulators like p53 and p21 in (B) Rg3(*S*)-treated old HDFs and (C) Rg3(*R*)-treated old HDFs. To compare relative expression levels, β-actin was used as loading control. HDF, human dermal fibroblast; PI3K, phosphatidylinositol 3-kinase.

ameliorate the senescence of human fibroblasts is highly notable. Thus, it is postulated that the mitochondrial biogenesis in old HDFs was augmented by the treatment with Rg3(*S*), leading to the restoration of mitochondrial function.

3.3. Rg3(S) decreases ROS level and increases NAD^+/NADH ratio in rotenone-stressed young HDFs

Generally, the redox status of NAD^+ and NADH plays key roles in regulation of catabolic processes, which is deeply linked to oxidative stress and antioxidant defense [35]. Further, we investigated whether Rg3(*S*) decreases the level of ROS and increases NAD/NADH ratio under artificial oxidative stress in young HDFs. We used rotenone, a naturally occurring plant-derived pesticide, to inhibit the activity of mitochondrial complex I and generate ROS in large quantities [36]. When 1 mM rotenone was applied to young HDFs, the amount of ROS increased to approximately 30%; however, Rg3(*S*) decreased the levels of ROS in rotenone-treated young HDFs in a dose-dependent manner (Fig. 5A). The intracellular NAD^+/NADH ratio in young HDFs stressed with rotenone was decreased to less than 1% of control cells. However, the NAD^+/NADH ratios in almost completely rotenone-reduced status of young HDFs were dramatically recovered to 2.7 (77% of control) and 3.0 (86% of control) upon treatment with 10 and 30 μM Rg3(*S*), respectively (Fig. 5B). These data indicate that Rg3(*S*) decreases the level of intracellular ROS and increases NAD^+/NADH ratios in rotenone-stressed young HDFs like senescent HDFs.

3.4. Rg3(S) specifically modulates AKT/mTOR signaling pathway in senescent HDFs

Based on the biochemical and molecular evidence of reversal effects of Rg3(*S*) on senescent HDFs, we investigated the signaling pathways regulated by Rg3(*S*) in senescent cells. Levels of key aging-related proteins such as AMPK, mTOR, p53/p21, and GSK3β in senescent HDFs were quantified and compared with those in Rg3(*S*)-treated old HDFs by immunoblot analysis. As shown in Fig. 6 and Supplementary Fig. 1, the protein levels of p-mTOR, p-GSK3β, cyclin D1, p16, p-p53, and p21 in old HDFs were significantly increased ($p < 0.001$) in comparison to those in young HDFs. However, the Rg3(*S*) treatment significantly downregulated the levels of aging-related proteins, as mentioned above. Contrary to these data, the protein levels of p-AMPK and Sirt1 ($p < 0.001$), Sirt3 (not significant), and Sirt6 ($p < 0.01$) in old HDFs were decreased in comparison to young HDFs (Figs. 4 and 6A). However, the Rg3(*S*) treatment significantly upregulated the protein levels of active

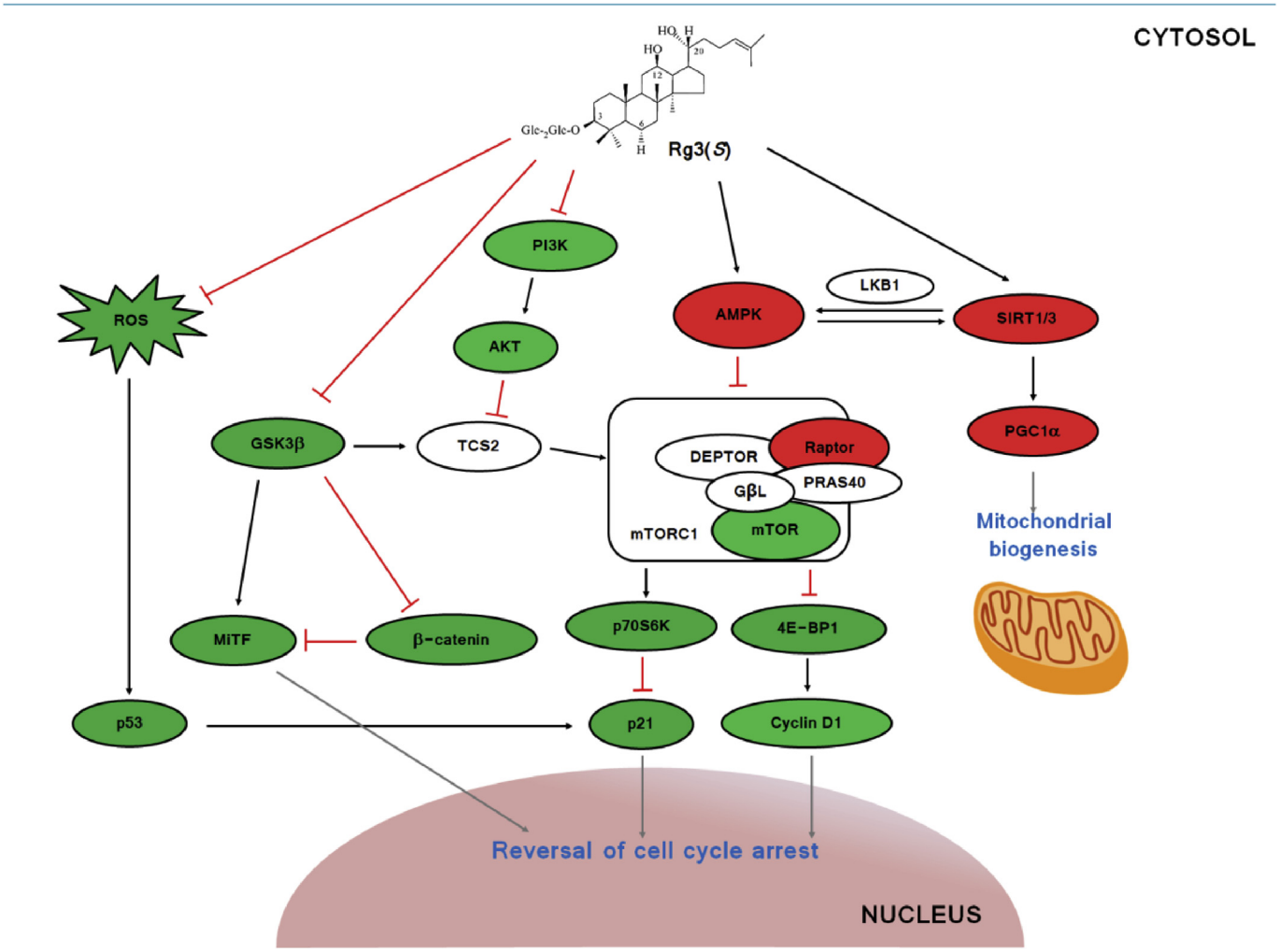

Fig. 7. Working model for the reversal effect of Rg3(*S*) on senescent HDFs. Green symbol represents the inactivation or decreasing expression of proteins and red symbol represents the activation or increasing expression of proteins, respectively, following treatment with Rg3(*S*) according to the above biochemical and immunoblot assays. White symbols were not checked in the present study. HDF, human dermal fibroblast; ROS, reactive oxygen species; PI3K, phosphatidylinositol 3-kinase.

AMPK and sirtuins. In our previous study, modified *P. ginseng*, including both R and S form of Rg3, increased pAkt and decreased mTOR-4EBP1 in lung cancer cells [37]. Furthermore, we investigated the stereoisomer-specific effects of Rg3 on the reversal of senescent cells. The levels of PI3K and p-Akt were significantly decreased by Rg3(*S*) in senescent HDFs, whereas Rg3(*R*) significantly increased the levels of these survival signaling-related proteins (Fig. 6B and C). Many literatures report the differential effects of stereoisomers of Rg3 in human keratinocyte and dermal fibroblasts [12]. Additionally, it was reported that total saponin from Korean Red Ginseng inhibits the binding of adhesive proteins to glycoprotein IIb/IIIa via phosphorylation of VASP at Ser-157 and dephosphorylation of PI3K and Akt [38]. It was also reported that ethanolic extract of *P. ginseng* calyx may exert NF-κB-targeting antiinflammatory properties through suppression of AKT [39]. It is suggested that the stereosiomeric ginsenosides Rg3(*S*) and Rg3(*R*) stimulate different signaling molecules in survival signaling in senescent HDFs.

Using data based on the immunoblot analyses (Figs. 3, 4 and 6, Suppl. Fig. 1), we present the working model of Rg3(*S*) on the senescent HDF cells (Fig. 7). Rg3(*S*) may function in multiple ways to activate Sirt1, Sirt3, and AMPK but suppress ROS, GSK3β, and PI3K. Cell cycle regulators like p21 and cyclin D1 affect the reversal of cell cycle arrest in senescent HDFs. In mitochondrial function, activated Sirt1 and, in particular, Sirt3 activates PGC1α to promote the biogenesis of mitochondria. Our observations match well with the previous report that PGCα and Sirtuin-3 play pivotal roles in mitochondrial function, such as mitochondrial DNA content, energy levels, and oxidative stress–like ROS [40]. Similarly, to the reversal effect of Rg3(*S*), it is well known that calorie restriction and resveratrol also increase mitochondrial biogenesis by the activation of PGC1α [41]. AMPK activated by Rg3(*S*) suppresses mTORC1, which upregulates Raptor and downregulates mTOR, thereby regulating downstream signaling molecules such as p70S6K and 4E-BP1. Downregulated survival signals such as PI3K and Akt inhibit TCS2 to presumably activate mTORC1. Downregulated Glycogen Synthase Kinase 3 Beta (GSK3β) regulates downstream signaling molecules (β-catenin, MiTF) differently, leading to the reversal of cell cycle arrest.

More detailed evidence of Rg3-mediated signaling pathways remains to be elucidated. These cellular molecular analyses will provide fruitful insight into the possibility of a therapeutic potential of Rg3(*S*) against replicative senescence of the aging process. Recently, it was summarized that several active ginsenosides, including Rg3(*S*), modulate neurodegenerative diseases by emerging signals in complicated signaling pathways. Therefore, further study of more systematic and in-depth efficacies and working mechanisms of active ginsenosides is required.

Conflicts of interest

All authors have no conflicts of interest to declare.

Acknowledgments

The present study was supported by the Korea Basic Science Institute research grant (C39712) awarded to J.S. Choi.

Appendix A. Supplementary data

Supplementary data to this article can be found online at https://doi.org/10.1016/j.jgr.2019.08.002.

References

[1] van Deursen JM. The role of senescent cells in ageing. Nature 2014;509:439–46.
[2] Hayflick L, Moorhead PS. The serial cultivation of human diploid cell strains. Exp Cell Res 1961;25:585–621.
[3] Davalli P, Mitic T, Caporali A, Lauriola A, D'Arca D. ROS, cell senescence, and novel molecular mechanisms in aging and age-related diseases. Oxid Med Cell Longev 2016;2016:3565127.
[4] Davinelli S, Bertoglio JC, Polimeni A, Scapagnini G. Cytoprotective polyphenols against chronological skin aging and cutaneous photodamage. Curr Pharm Des 2018;24:99–105.
[5] Sarubbo F, Moranta D, Asensio VJ, Miralles A, Esteban S. Effects of resveratrol and other polyphenols on the most common brain age-related diseases. Curr Med Chem 2017;24:4245–66.
[6] Oh SJ, Kim K, Lim CJ. Protective properties of ginsenoside Rb1 against UV-B radiation-induced oxidative stress in human dermal keratinocytes. Pharmazie 2015;70:381–7.
[7] Fernandez-Moriano C, Gonzalez-Burgos E, Iglesias I, Lozano R, Romez-Serranillos MP. Evaluation of the adaptogenic potential exerted by ginsenosides Rb1 and Rg1 against oxidative stress-mediated neuroptoxicity in an in vitro neuronal model. PLoS One 2017;12:e0182933.
[8] Mohanan P, Subramaniyam S, Mathiyalagan R, Yang DC. Molecular signaling of ginsenosides Rb1, Rg1, and Rg3 and their mode of actions. J Ginseng Res 2018;42:123–32.
[9] Guo M, Guo G, Xiao J, Sheng X, Zhang X, Tie Y, Cheng YK, Ji X. Ginsenoside Rg3 stereoisomers differentially inhibit vascular smooth muscle cell proliferation and migration in diabetic athereosclerosis. J Cell Mol Med 2018;22:3202–14.
[10] Park MW, Ha J, Chung SH. 20(S)-ginsenoside Rg3 enhances glucose-stimulated insulin secretion and activates AMPK. Biol Pharm Bull 2008;31:748–51.
[11] Wei X, Chen J, Su F, Su X, Hu T, Hu S. Stereospecificity of ginsenoside Rg3 in promotion of the immune response to ovalbumin in mice. Int Immunol 2012;24:465–71.
[12] Lim CJ, Choi WY, Jung HJ. Stereoselective skin anti-photoaging properties of ginsenoside Rg3 in UV-B irradiated keratinocytes. Biol Pharm Bull 2014;37:1583–90.
[13] Theurey P, Pizzo P. The aging mitochondria. Genes (Basel) 2018;9:E22.
[14] Sahin E, DePino RA. Axis of ageing: telomeres, p53 and mitochondria. Nat Rev Mol Cell Biol 2012;13:397–404.
[15] Rodgers JT, Lerin C, Haas W, Gygi SP, Spiegelman BM, Puigserver P. Nutrient control of glucose homeostasis through a complex of PGC-1alpha and Sirt1. Nature 2005;434:113–8.
[16] Tao R, Coleman MC, Pennington JD, Ozden O, Park SH, Jiang H, Kim HS, Flynn CR, Hill S, Hayes McDonald W, et al. Sirt3-mediated deacetylation of evolutionarily conserved lysine 122 regulates MnSOD activity in response to stress. Mol Cell 2010;40:893–904.
[17] Spadari RC, Cavadas C, de Carvalho AETS, Ortolani D, De Moura AL, Vassalo PF. Role of beta-adrenergic receptors and sirtuin signaling in the heart during aging, heart failure, and adaptation to stress. Cell Mol Neurobiol 2018;38:109–20.
[18] Hu D, Cao S, Zhang G, Xiao Y, Liu S, Shang Y. Florfenicol-induced mitochondrial dysfunction suppresses cell proliferation and autophagy in fibroblasts. Sci Rep 2017;7:13554.
[19] Jang IS, Jo E, Park SJ, Hwang IH, Kang HM, Lee JH, Kwon J, Son J, Kwon HJ, Choi JS. Proteomic analyses reveal that ginsenoside Rg3(S) partially reverses cellular senescence in human dermal fibroblasts by inducing peroxiredoxin. J Ginseng Re 2019. https://doi.org/10.1016/j.jgr.2018.07.008.
[20] Dimri GP, Lee X, Basile G, Acosta M, Scott G, Roskelley C, Medrano EE, Linskens M, Rubelj I, Pereira-Smith O. A biomarker that identifies senescent human cells in culture and in aging skin in vivo. Proc Natl Acad Sci USA 1995;92:9363–7.
[21] Eruslanov E, Kusmartsev S. Identification of ROS using oxidized DCFDA and flow-cytometry. Methods Mol Biol 2010;594:57–72.
[22] Quispe-Tintaya W, White RR, Popov VN, Vijg J, Maslov AY. Fast mitochondrial DNA isolation from mammalian cells for nex-generation sequencing. Biotechniques 2013;55:133–6.
[23] Stein GH, Dulic V. Molecular mechanisms for the senescent cell cycle arrest. J Invest Dermatol Symp Proc 1998;3:14–8.
[24] Chen C, Mu XY, Zhou Y, Shun K, Geng S, Liu J, Wang JW, Chen J, Li TY, Wang YP. Ginsenoside Rg1 enhances the resistance of hematopoietic stem/progenitor cells to radiation-induced aging in mice. Acta Pharmacol Sin 2014;35:143–50.
[25] Chen X, Wang M, Xu X, Liu J, Mei B, Fu P, Zhao D, Sun L. *Panax ginseng* total protein promotes proliferation and secretion of collagen in NIH/3T3 cells by activating extracellular signal-related kinase pathway. J Ginseng Res 2017;41:411–8.
[26] Lee JO, Kim E, Kim JH, Hong YH, Kim HG, Jeong D, Kim J, Kim SH, Park C, Seo DB, et al. Antimelanogenesis and skin-protective activities of *Panax ginseng* calyx ethanol extract. J Ginseng Res 2018;42:389–99.
[27] McBride HM, Neuspiel M, Wasiak S. Mitochondria: more than just a powerhouse. Curr Biol 2006;16:R551–60.

[28] Wiley CD, Campisi J. From ancient pathways to aging cells – connecting metabolism and cellular senescence. Cell Metab 2016;23:1013–21.
[29] James EL, Michalek RD, Pitiyage GN, de Castro AM, Vignola KS, Jones J, Mohney RP, Karoly ED, Prime SS, Parkinson EK. Senescent human fibroblasts show increased glycolysis and redox homeostasis with extracellular metabolomes that overlap with those of irreparable DNA damage, aging, and disease. J Proteome Res 2015;14:1854–71.
[30] Chen X, Zhang J, Fang Y, Zhao C, Zhu Y. Ginsenoside Rg1 delays tert-butyl hydroperoxide-induced premature senescence in human WI-38 diploid fibroblast cells. J Gerontol A Biol Sci Med Sci 2008;63:253–64.
[31] Blacker TS, Duchen MR. Investigating mitochondrial redox state using NADH and NADPH autofluorescence. Free Radic Biol Med 2016;100:53–65.
[32] Yang JL, Ha TK, Dhodary B, Kim KH, Park J, Lee CH, Kim YC, Oh WK. Dammarane triterpenes as potential SIRT1 activators from the leaves of Panax ginseng. J Nat Prod 2014;77:1615–23.
[33] Song Z, Liu Y, Hao B, Yu S, Zhang H, Liu D, Zhou B, Wu L, Wang M, Xiong Z, et al. Ginsenoside Rb1 prevents H2O2-induced HUVEC senescence by stimulating sirtuin-1 pathway. PLoS One 2014;9:e112699.
[34] Kim MJ, Koo YD, Kim M, Lim S, Park YJ, Chung SS, Jang HC, Park KS. Rg3 improves mitochondrial function and the expression of key genes involved in mitochondrial biogenesis in C2C12 myotubes. Diabetes Metab J 2016;40:406–13.
[35] Raha S, Robinson BH. Mitochondria, oxygen free radicals, disease and ageing. Trends Biochem Sci 2000;25:502–8.
[36] Ueno H, Miyoshi H, Ebisui K, Iwamura H. Comparison of the inhibitory action of natural rotenone and its stereosiomers with various NADH-ubiquinone reductases. Eur J Biochem 1994;225:411–7.
[37] Yoo HS, Kim JM, Jo E, Cho CK, Lee SY, Kang HS, Lee MG, Yang PY, Jang IS. Modified Panax ginseng extract regulates autophagy by AMPK signaling in A547 human lung cancer cells. Oncol Rep 2017;37:3287–96.
[38] Kwon HW, Shin JH, Cho HJ, Rhee MH, Park HJ. Total saponin from Korean Red Ginseng inhibits binding of adhesive proteins to glycoprotein IIb/IIIa via phosphorylation of VASP (Ser(157)) and dephosphorylation of PI3K and Akt. J Ginseng Res 2016;40:76–85.
[39] Han SY, Kim J, Kim E, Kim SH, Seo DB, Kim JH, Shin SS, Cho JY. AKT-targeted anti-inflammatory activity of Panax ginseng calyx ethanolic extract. J Ginseng Res 2018;42:496–503.
[40] Lopez-Lluch G, Irusta PM, Navas P, de Cabo R. Mitochondrial biogenesis and healthy aging. Exp Gerontol 2008;43:813–9.
[41] Rato L, Duarte AI, Tomas GD, Santos MS, Moreira PI, Socorro S, Cavaco JE, Alves MG, Oliverira PF. Pre-diabetes alters testicular PGC1-α/SIRT3 axis modulating mitochondrial bioenergetics and oxidative stress. Biochim Biophys Acta 2014;1837:335–44.